



U-Th stratigraphy of a cold seep carbonate crust

G. Bayon, G.M. Henderson, Marcel Bohn

► To cite this version:

G. Bayon, G.M. Henderson, Marcel Bohn. U-Th stratigraphy of a cold seep carbonate crust. Chemical Geology, 2009, 260 (1-2), pp.47-56. 10.1016/j.chemgeo.2008.11.020 . insu-00377423

HAL Id: insu-00377423

<https://hal-insu.archives-ouvertes.fr/insu-00377423>

Submitted on 26 Jun 2012

HAL is a multi-disciplinary open access archive for the deposit and dissemination of scientific research documents, whether they are published or not. The documents may come from teaching and research institutions in France or abroad, or from public or private research centers.

L'archive ouverte pluridisciplinaire **HAL**, est destinée au dépôt et à la diffusion de documents scientifiques de niveau recherche, publiés ou non, émanant des établissements d'enseignement et de recherche français ou étrangers, des laboratoires publics ou privés.

U–Th stratigraphy of a cold seep carbonate crust

G. Bayon^{a,*}, G.M. Henderson^b & M. Bohn^c

^a Département Géosciences Marines, Ifremer, 29280 Plouzané, France

^b Department of Earth Sciences, Oxford University, Parks Road, OX1 3PR Oxford, UK

^c Microsonde Ouest, CNRS-UMR 6538, Ifremer, 29280 Plouzané, France

*: Corresponding author : Germain.Bayon@ifremer.fr

Abstract:

On continental margins, oxidation of methane-rich fluids from the sediment often leads to formation of authigenic carbonate pavements on the seafloor. The biogeochemical processes involved during this carbonate precipitation are increasingly understood, but little is known about the duration or mode of carbonate crust formation. Here, we report uranium and thorium concentrations and isotope compositions for a set of 14 samples drilled across an authigenic carbonate pavement, which provide the first stratigraphy for a cold-seep carbonate crust. The 5.5-cm thick crust (NL7-CC2) was collected by submersible on the Nile deep-sea fan in an area of active fluid venting. U–Th analyses must be corrected for initial Th and measurement of co-existing sediments indicates the presence of both scavenged and detrital initial ^{230}Th , which must be considered during this correction. The calculated $^{230}\text{Th}/\text{U}$ age-depth profile for NL7-CC2 provides evidence for continuous downward carbonate precipitation at the studied location over the last ~ 5000 years. Three distinct phases can be distinguished from top to bottom with average growth rates of ~ 0.4, 5 and 0.8 cm/kyr, respectively, corresponding to carbonate precipitation rates ranging from ~ 7 to 92 $\mu\text{mol m}^{-2} \text{h}^{-1}$ (rates consistent with previous estimates). High-resolution $\delta^{13}\text{C}$ profiles [Gontharet, S., Pierre, C., Blanc-Valleron, M.- M., Rouchy, J.M., Fouquet, Y., Bayon, G., Foucher, J.P., Woodside, J., Mascle, J., The Nautinil Scientific Party, 2007. Nature and origin of diagenetic carbonate crusts and concretions from mud volcanoes and pockmarks of the Nile deep-sea fan (eastern Mediterranean Sea). *Deep Sea Res. II* 54, 1292–1311] and major elements across NL7-CC2 show that the variations in carbonate precipitation rates were also accompanied by changes in carbonate mineralogy and fluid composition. We suggest that these changes primarily reflect modification of the diagenetic environment, i.e. a progressive depletion of dissolved sulphate through anaerobic oxidation of methane, caused by the initial carbonate crust formation and the resulting reduction in bioirrigation. Overall, U–Th dating of cold seep carbonates offers a promising tool to bring new insights into biogeochemical processes at cold seeps and to assess the timing and duration of fluid venting on continental margins.

1. Introduction

Cold seep carbonates are a promising archive of past fluid flow and gas hydrate dissociation on continental margins. They typically form in sub-surface sediments at cold seeps, resulting from the microbial oxidation of methane-rich fluids (e.g. Ritger et al., 1987; Hovland et al., 1987; Paull et al., 1992; Bohrmann et al., 1998; Aloisi et al., 2000, 2002; Greinert et al., 2001; Michaelis et al., 2002; Mazzini et al., 2004; Reitner et al., 2005; Stadnitskaia et al., 2005; Gontharet et al., 2007). In fluid venting areas, anaerobic oxidation of methane (AOM) leads to enhanced alkalinity and dissolved sulphide contents in pore waters, which favours carbonate precipitation and the development of chemosynthetic communities on the seafloor.

In many settings, carbonate precipitation forms a hard crust at the sediment surface. Numerical modelling indicate that such carbonate crusts may form within a time period of several centuries (Luff and Wallmann, 2003; Luff et al., 2004, 2005), but these estimates of growth rate and duration have not been confirmed with chronological observations and little is known about the effect of crust growth on fluid venting. To address these questions requires establishing an accurate chronology for crust formation. This cannot be achieved using radiocarbon techniques because cold-seep carbonates derive part of their carbon from old sources (i.e. methane). A few previous studies have demonstrated that U-series could be used successfully to date cold seep carbonates from modern fluid venting systems (Lalou et al., 1992; Teichert et al., 2003; Watanabe et al., 2008), but there has been no detailed investigation of crust formation at a single site to allow reconstruction of paleo-methane seepage history at a high-resolution temporal scale.

The major difficulty in dating cold-seep carbonates is that they often incorporate a significant fraction of detrital sediment (e.g. clays), which represents a major source of initial ^{230}Th (i.e. not produced by *in situ* decay). Such detrital ^{230}Th is accompanied by a much larger amount of ^{232}Th , because the $^{230}\text{Th}/^{232}\text{Th}$ ratio in most geological materials is $\sim 5 \times 10^{-6}$. A typical correction procedure for dating dirty carbonates is the measurement of the isotopic composition of the contaminating phase (i.e. sediment) using isochron techniques (e.g. Luo and Ku, 1991; Bischoff and Fitzpatrick, 1991; Edwards et al., 2003). Isochron methods consider each sample to be composed of a mixture of two components and are used to separate ^{230}Th present initially (i.e. detrital ^{230}Th) from that ingrown from U in the carbonate. Concern may arise however when more than one component of initial thorium exists in the carbonate samples, each with

its own $^{230}\text{Th}/^{232}\text{Th}$ ratios (Lin et al., 1996). This is the case when carbonates contain a source of ^{230}Th scavenged from seawater, in addition to detrital ^{230}Th and radiogenic ^{230}Th (Lin et al., 1996; Henderson et al., 2001). Hence, the origin of initial ^{230}Th in any cold seep carbonate samples must be distinguished in order to obtain reliable age information with isochron methods.

In this study, we present the first high-resolution stratigraphy for a cold-seep carbonate crust. U-Th carbonate age data were acquired on a series of samples drilled across a carbonate pavement from the Nile deep-sea fan. The U-Th age-depth profile is used together with $\delta^{13}\text{C}$ (Gontharet et al., 2007) and major element data to determine carbonate precipitation rates and to provide new insights on the factors affecting crust formation at cold seeps.

2. Description of NL7-CC2 crust

The carbonate crust analysed in this study was recovered offshore Egypt by submersible during the Nautinil expedition (RV Atalante, 2003), on the Nile deep-sea fan (Eastern Mediterranean basin; Fig. 1). Crust NL7-CC2 was collected from a large ($>1\text{ km}^2$) carbonate-paved area associated with chemosynthetic vent communities at $\sim 1650\text{ m}$ water depth (Fig. 2A; Bayon et al., In press). It is a $\sim 5.5\text{ cm}$ -thick, highly porous, carbonate-cemented mudstone, covered by a fine layer of Fe-oxyhydroxides (Fig. 2B). The bulk crust density is 1.6 g cm^3 . Gontharet et al. (2007) showed that crust NL7-CC2 is dominated by aragonite, but exhibits mineralogical variability, characterized by a gradual enrichment in high-Mg carbonate phases from top to bottom (Fig. 2B). Examination of NL7-CC2 under optical and scanning electron microscopes shows that this change from aragonite to calcite is not due to aragonite recrystallisation (Gontharet et al., 2007). The $\sim 1\text{-cm}$ top part of the crust is composed of various fragments of chemosynthetic bivalve shells (Vesycomyidae and Thyasiridae; Bayon et al., In press), cemented by aragonite (Fig. 2B). Upon recovery, numerous living vestimentiferan tubeworms were observed anchored at the base of the crust, which indicate that active fluid venting occurs at that site (Fig. 2A). Fibrous aragonite is present typically in open pore spaces, either in cracks or inside the cavities of biogenic components (e.g. foraminifers, bivalve shells).

3. Analytical techniques

3.1. Electron microprobe analysis and XRF

Polished sections of crust NL7-CC2 were examined by scanning electron microscopy (JEOL JSM-840A, University of Oxford) to select sampling areas suitable for U-Th measurements based on the texture of carbonate growth. To assess the bulk major element composition, five ~1-cm-thick slices sampled across a section of NL7-CC2 crust were analysed by wavelength-dispersive X-ray fluorescence (WD-XRF) analysis of fusion beads. These analyses were performed on the same powders analysed for mineralogy and $\delta^{13}\text{C}$ by Gontharet et al. (2007). In addition, high-resolution abundance profiles of Ca, Mg, Sr, Si, Al, Ti, Fe, K, P, Mn, C and O were measured by electron microprobe (Cameca SX50, Microsonde Ouest, IFREMER) on one thin section of NL7-CC2 crust cross cut perpendicular to its growth banding. Analyses were made using an accelerating voltage of 15 kV and a beam current of 10 nA. Spot analyses of the crusts were made at a resolution of 0.1 mm with a 20 μm beam diameter. The relative error for each element is approximately 1% (1σ) for concentrations in the range 10–30 wt%, but increases to about 10% (1σ) for concentrations between 0.1 and 0.5 wt%. The porous nature of the crust, and the fact that both C and O were measured during analysis, resulted in oxide totals mostly higher than 105%. Analyses with totals more than 115% were rejected and other analyses were normalized to a 100% total. For both XRF and electron microprobe data, detrital contents along the crust were estimated simply by summing contents of K_2O , Fe_2O_3 , SiO_2 , TiO_2 and Al_2O_3 .

3.2. Sampling, chemical and analytical procedures for U-Th measurements

Selected areas of carbonate crust were hand-drilled carefully to obtain samples of between ~ 50-500 mg. Carbonate samples were collected at different depths across a cross-cut section of NL7-CC2 crust. Carbonate crusts are typically highly heterogeneous and samples of this size (referred to as ‘bulk’ samples in the following text) are contaminated by detrital material, complicating U-Th dating. To try to reduce such contamination, some carbonate samples were also collected using a computer-assisted microsampling device (MicroMill, New Wave Research). This system

enables accurate sampling of sub-millimeter areas of polished sections. For those small carbonate samples (referred to as ‘micromilled’ samples subsequently), sampling areas were selected using scanning electron microscopy and/or electron microprobe analyzer. Great care was taken to avoid sampling of detrital grains (i.e. quartz), biogenic components and cavities (e.g. fossil emplacements of tubeworms), which may be filled with late-stage aragonite (Fig. 1). About ~ 1 mg of carbonate powder was collected for each of those micromilled samples for U-Th analysis.

To assess the composition of the detrital end-member and thereby allow an isochron approach, two sediment samples were analysed which were collected using submersible-mounted corers in the studied area, but away from active zones of fluid seepage. These samples - NL14-PC1 and NL7-BC1 - were recovered at ~ 2120m and 1620m water depths, respectively, and are reddish-brown foraminiferal and pteropod oozes. The average of their U-series composition was assumed to be representative of the sediment fraction incorporated within the carbonate crust.

Each sample (i.e. bulk, micromilled, sediment) was dissolved slowly in 7.5M HNO₃ and spiked with a mixed ²³⁶U/²²⁹Th spike (Robinson et al., 2002). Any undissolved detrital fractions were transferred into cleaned Teflon vessels and fully digested with a mixed (3:1) HF:HCl solution before being added back into corresponding supernatants. Samples were evaporated, taken up with 7.5M HNO₃, and diluted with ultrapure water. U and Th were then co-precipitated onto Fe-oxides after addition of 5 mg (2.5 mg for micromilled samples) of ultrapure Fe and precipitation with ammonia. After 24 hours, Fe-oxides were centrifuged, cleaned several times in ultrapure water and dissolved in 7.5M HNO₃. Finally, U and Th were separated chemically using conventional anion exchange techniques adapted from previous studies (Edwards et al., 1986). The volumes of anion-exchange resin and acids used for separating U-Th were much smaller for micromilled samples than for bulk and sediment samples. Typical procedural blanks were 1.2x10⁻¹⁰ g ²³⁸U and 3.0x10⁻¹¹ g ²³²Th for bulk carbonate and sediment samples, and 1.0x10⁻¹¹ g ²³⁸U and 1.3x10⁻¹² g ²³²Th for micromilled samples. Total U and Th procedural blanks were small compared to final sample concentrations.

U and Th concentrations and isotope ratios were measured with a MC-ICPMS (Nu Plasma). Procedures largely follow those described in Robinson et al. (2002). The

external reproducibility on the $^{234}\text{U}/^{235}\text{U}$ ratio was assessed by repeatedly measuring the CRM-145 standard during each session using a standard-bracketing measurement protocol (Robinson et al., 2002), and was 1.7 ‰ (2 s.d.) for sediment and bulk carbonate samples and ranged from 2.7 to 8.3 ‰ for the mg-sized carbonate samples. Th was measured with ^{229}Th and ^{230}Th sequentially in a single ion-counter equipped with an energy filter to improve abundance sensitivity, and ^{232}Th in a Faraday collector. Mass discrimination and ion-counter gain were assessed by bracketing Th samples with CRM-145 U measurements. Internal precision obtained on measured $^{229}\text{Th}/^{230}\text{Th}$ ratios was always better than 5 ‰ for sediment and bulk carbonate samples, and better than 50 ‰ for the smaller micromilled samples. Previous assessment of this measurement approach using TIMS calibrated in-house Th standards (e.g. Robinson et al. 2002) has indicated its accuracy, and that internal precisions are a reasonable assessment of external repeatability at the low signal intensities used in this study.

Carbonate ages were corrected for detrital contamination by assuming that the mean composition of the modern local sediment well represents the initial detrital component for all samples. Ages were calculated from the measured ($^{232}\text{Th}/^{238}\text{U}$), ($^{230}\text{Th}/^{238}\text{U}$), ($^{234}\text{U}/^{238}\text{U}$) of each sample and these ratios in the average sediment value using a two-point isochron approach, calculated in 3D using the ISOPLOT program (v. 3.34, Ludwig, 2003) and half lives following Cheng et al. (2000), $\lambda_{230\text{Th}} = 9.158 \times 10^{-6} \text{ yr}^{-1}$, $\lambda_{232\text{Th}} = 4.95 \times 10^{-11} \text{ yr}^{-1}$, $\lambda_{234\text{U}} = 2.826 \times 10^{-6} \text{ yr}^{-1}$ and $\lambda_{238\text{U}} = 1.551 \times 10^{-10} \text{ yr}^{-1}$. Uncertainty in the isotopic composition of the sediment end-member was assumed to correspond to the standard deviation (2SD) of the measured ($^{232}\text{Th}/^{238}\text{U}$), ($^{230}\text{Th}/^{238}\text{U}$) and ($^{234}\text{U}/^{238}\text{U}$) activity ratios for the two sediments analysed.

4. Results

4.1. Major element data

Electron microprobe Sr/Ca ratios vary from ~ 0.001 to 0.040, and Mg/Ca ratios from 0.0 to 0.3 (Fig. 3A,B). Down-crust variation of Sr/Ca and Mg/Ca is due to changes in mineralogy, being controlled by the relative contribution of Sr-rich aragonite, Mg-rich carbonate phases, low-Mg calcite, and detritus (Bayon et al., 2007). Sr/Ca ratios are most typically around 0.020, which indicates the predominance of aragonite in the

crust (Bayon et al., 2007). Sr/Ca and Mg/Ca values are both low in the upper part of the studied section (i.e. the top 0.4 cm) reflecting the presence of low-Mg calcite in the bivalve shells (Fig. 3B). Below this upper layer, the frequency of high Mg/Ca values increases progressively with depth, indicating enhanced contribution from high-Mg carbonate phases. Detrital contents in crust NL7-CC2, inferred from both electron microprobe and XRF data (Table 1), can be as high as ~ 12 wt%, increasing progressively with depth (Fig. 3C).

4.2. U-series data

Uranium concentrations vary from ~ 1 to 20 ppm for carbonate samples (bulk and micromilled) and average 1.3 ppm in the two sediment samples (Table 2). These carbonate concentrations are comparable to those reported in the literature for other cold seep carbonates (Teichert et al., 2003; Watanabe et al., 2008). The average ^{238}U concentration in crust NL7-CC2 increases progressively with depth, from ~3.5 ppm for the uppermost centimetre, to ~9.6 ppm for the middle part (from 1 cm to 4.3 cm-depth) and ~20.8 ppm for the bottom part of the crust.

^{232}Th concentrations range from ~30 to 2100 ppb in carbonates and are 4200 and 5000 ppb in the two sediments. Carbonate ($^{230}\text{Th}/^{232}\text{Th}$) ratios are low compared to many natural carbonates (from 2.6 to 11.5, Table 2), due to the young age (low ^{230}Th ingrowth), but also, more importantly, to detrital contamination (high initial ^{232}Th). The mean ($^{238}\text{U}/^{232}\text{Th}$) value for the two sediments is 0.87 ± 0.02 , which is typical of detrital sediments and river suspended particles (e.g. Vigier et al., 2001; Ludwig and Paces, 2002; Dosseto et al., 2006a,b). Sediment ($^{230}\text{Th}/^{232}\text{Th}$) ratios are significantly higher (~2.3) than secular equilibrium (Table 3), due to addition of excess ^{230}Th from seawater.

On a ($^{230}\text{Th}/^{232}\text{Th}$) vs. ($^{238}\text{U}/^{232}\text{Th}$) isochron diagram (i.e. a Rosholt-type diagram), the carbonate samples from crust NL7-CC2 plot well within the range of published data for other cold seep carbonates (Fig. 4B). Micromilled carbonate samples exhibit ($^{230}\text{Th}/^{232}\text{Th}$) and ($^{238}\text{U}/^{232}\text{Th}$) ratios higher than bulk carbonate crust samples (Fig 4A) indicating that micromilling has been successful, to some extent, in separating carbonate phases from detrital-rich areas within carbonate crust. For all the carbonate samples reported in this study, however, both major element and U-Th data clearly

show that detrital contamination is too high to allow calculation of simple $^{230}\text{Th}/\text{U}$ ages, and a correction for initial detrital content is required.

Measured ($^{234}\text{U}/^{238}\text{U}$) ratios (Table 2) are quoted as initial $\delta^{234}\text{U}$ values, corrected for detrital contamination and decay of excess ^{234}U since sample formation (Table 3), where $\delta^{234}\text{U}$ represents the deviation in permil of ($^{234}\text{U}/^{238}\text{U}$) from its secular equilibrium value of 1.000: $\delta^{234}\text{U} = [\{ (^{234}\text{U}/^{238}\text{U})_{\text{meas}} / (^{234}\text{U}/^{238}\text{U})_{\text{equ}} \} - 1] \times 10^3$. Initial $\delta^{234}\text{U}$ values range from 130 to 153, and all samples exhibit, within error, values close to modern seawater (146.6 ± 2.5 ‰; Robinson et al., 2004). This indicates that the carbonate bound U is likely to be derived from seawater rather than from pore waters; this latter U-pool being typically characterized by much higher $\delta^{234}\text{U}$ (Cochran et al., 1986; Gariepy et al., 1993; Henderson et al., 1999).

5. Discussion

5.1. Detrital versus hydrogenous source of initial ^{230}Th

The high ($^{230}\text{Th}/^{232}\text{Th}$) ratios measured in sediments provide clear evidence for two possible sources of initial ^{230}Th : supported ^{230}Th within the detrital grains, and excess ^{230}Th scavenged to the grain-surfaces from seawater. Any assumption that initial Th has a typical crustal ($^{230}\text{Th}/^{232}\text{Th}$) would therefore lead to errors in calculated ages. This indicates the need to measure the sediment end-member directly to improve age accuracy when dating carbonate crusts.

The presence of two sources of initial ^{230}Th raises the possibility that the mixture of these two sources might change with time, making the use of a constant initial composition inappropriate. Changes in the ($^{230}\text{Th}/^{232}\text{Th}$) of the sediment material accumulating on the seafloor may occur. However, ^{230}Th is scavenged rapidly after its formation in seawater (Henderson et al. 1999), so the flux of ^{230}Th to the sediment should remain largely unchanged at any one site. Significant changes in the flux of detrital ^{232}Th would therefore be required to alter the sedimenting ($^{230}\text{Th}/^{232}\text{Th}$) and, although these may occur on longer timescales, they are unlikely within the Holocene period in which crust NL7-CC2 grew. Another issue is that after carbonate precipitation and incorporation of the sediment in the crust, the ^{230}Th excess in the

sediment component then starts to decay towards equilibrium. Formally, this would need to be corrected for the age calculation. However, because the studied carbonate samples are relatively young, the decay of sediment-bound ^{230}Th is small compared to the existing 2s uncertainty on the ($^{230}\text{Th}/^{232}\text{Th}$) value for the sediment end-member, and hence, can be neglected.

A potentially more significant mechanism to alter the mixture of detrital and scavenged Th initially present is by the direct scavenging of seawater Th to the crust surface. Some assessment of the magnitude of this process can be derived by considering the ^{232}Th budget of the crust samples. By assuming that ^{232}Th in each sample is entirely within detrital particles, a maximum ^{232}Th concentration of the detrital particles can be calculated for each sample. This calculation is performed using detrital fractions calculated with the bulk chemical data for each sample (Fig. 3C) and measured ^{232}Th concentrations (Table 2). The calculation indicates maximum detrital ^{232}Th concentrations for all but the uppermost sample of ~ 6 to 20 ppm. This range is in good agreement with the detrital Th contents of the two studied sediment samples (~15 ppm, as estimated on a carbonate-free basis; Table 1), and close to average shale composite Th concentrations (12.3 ppm for NASC - Condie, 1993; 14.6 ppm for PAAS - Taylor and McLennan, 1985). This suggests that there is negligible additional scavenging of ^{232}Th directly to the crust, and that correction for seawater-derived ^{232}Th is not necessary. The exception is the uppermost crust sample (0 cm) which yields an estimated maximum detrital ^{232}Th concentration of ~ 175 ppm, much higher than typical for crustal detritus. This suggests significant scavenging of Th to the crust surface directly from seawater. Hydrogenous Fe-oxide deposits are typically highly enriched in Th (e.g. Henderson and Burton 1999) and the Fe-oxide layer covering NL7-CC2 probably hosts this seawater-derived Th. Using simple mass balance considerations, the proportion of the hydrogenous component in the uppermost carbonate sample and its Th isotopic composition can be calculated (see Appendix for details of calculation). This calculation indicates that the hydrogenous Fe-oxide component is characterized by a ($^{230}\text{Th}/^{232}\text{Th}$) ratio of ~ 3.1, in agreement with activity ratios measured in the western Mediterranean Sea at similar water depths (Roy-Barman et al., 2002). It also shows that ~ 60% of ^{232}Th in the uppermost crust sample has been scavenged from seawater, whereas the remaining ~ 40% derives from sediment incorporated within the carbonate matrix (see Appendix).

Clearly, the isochron age calculated for the topmost sample (9.2 ± 2.5 ka; Table 1) is overestimated due to presence of initial hydrogenous ^{230}Th and, hence, is discarded in the discussion below. The ^{232}Th budget calculations suggest however that other crust samples have not been exposed significantly to seawater scavenging.

5.2. Validity of calculated ages and age uncertainties

The age calculated for the base of the NL7-CC2 crust using the high $^{230}\text{Th}/^{232}\text{Th}$ value of local sediment to correct for initial Th is 0.8 ± 1.3 ka (Table 3), which suggests that carbonate precipitation, and hence fluid seepage, is probably still active at the studied site. This agrees with evidence that dense bushes of vestimentiferan tubeworms live at present underneath carbonate pavements in this area (Bayon et al., In press), providing re-assurance for the validity of the dating approach, and for the suitability of the sediment end-member values used for calculations. Using an end-member with typical crustal values, i.e. at secular equilibrium, would lead instead to a much older age of ~ 5.2 kyr BP for the base of the carbonate crust, in contradiction with in situ observation.

The two-point isochron method used in this study is convenient for acquiring a high-resolution age profile for such ‘complex’ carbonate archives. However, the uncertainty in the ages calculated with this method depends crucially on the errors assigned to the sediment end-member used for calculations. In this study, the uncertainty in the end-member isotopic composition was taken as the standard deviation (2SD) of the isotope ratios measured for the two sediments analysed. For the ($^{230}\text{Th}/^{232}\text{Th}$) sediment ratio, this corresponds to a value of 2.31 ± 0.46 . Considering a less conservative error ($\pm 1\text{SD}$) on the sediment U/Th ratios would lead to smaller error bars on calculated isochron ages, such as 2.12 ± 0.84 ka for the sample drilled at 1cm-depth (instead of 2.1 ± 1.5 ka), and 0.84 ± 0.64 ka for the sample drilled at 5 cm-depth (instead of 0.8 ± 1.3 ka).

In order to further assess the suitability of our sediment end-member for calculating isochron ages, its composition was determined indirectly by performing additional 3-D isochron calculations on several sets of carbonate samples drilled at similar depths of

NL7-CC2 crust (hence assumed to have a similar age). This approach uses the intercept of each isochron to calculate the ^{232}Th -free ratios of ($^{230}\text{Th}/^{238}\text{U}$) and ($^{234}\text{U}/^{238}\text{U}$) required for the age calculation, but also estimates the present-day ($^{230}\text{Th}/^{232}\text{Th}$) ratio of the detrital sediment end-member. The isochron derived for the two bottommost samples of the crust, drilled at 5 cm and 5.5 cm-depth, yields a sediment end-member with ($^{230}\text{Th}/^{232}\text{Th}$) = 2.2 ± 0.4 (2SD). Another isochron was derived for the samples drilled at 3.6 cm and 4.3 cm-depth, which provides a ($^{230}\text{Th}/^{232}\text{Th}$) of 2.4 ± 1.0 . Finally, the isochron derived for the three samples collected at ~2.5 cm-depth gives a detrital ($^{230}\text{Th}/^{232}\text{Th}$) of 1.92 ± 0.12 . All those independently calculated ($^{230}\text{Th}/^{232}\text{Th}$) ratios agree well with the mean ($^{230}\text{Th}/^{232}\text{Th}$) \pm 2SD value obtained from the analysis of our two sediments (2.31 ± 0.46), providing further reassuring evidence for the suitability of the sediment end-member values and associated errors used for calculations. This shows that the two-point isochron ages calculated with our approach can be considered as robust.

5.3. U-Th isotope stratigraphy

The $^{230}\text{Th}/\text{U}$ age-depth profile for NL7-CC2 shows that the carbonate crust has grown downward since about 5 ± 1 ka (Fig. 3E). Previous studies suggested on theoretical grounds that carbonate crusts at cold seeps may grow downward into the sediment (Paull et al., 1992; Greinert et al., 2002; Aloisi et al., 2002), but our results represent the first direct evidence for this mode of formation. The average growth rate for crust NL7-CC2 is ~ 1.1 cm/kyr. In detail, however, three distinct periods of carbonate formation can be distinguished from top to bottom, with average growth rates of ~ 0.4 cm/kyr for the upper first centimetre, ~ 5 cm/kyr for the next four cm, and 0.8 cm/kyr for the bottom cm of the crust, respectively (Fig. 3E).

As discussed earlier, the relatively large error bars associated to calculated carbonate ages (on average ± 1.3 kyr; Table 3), reflect the large uncertainty on the sediment end-member composition. However, although the ($^{230}\text{Th}/^{232}\text{Th}$) of the sediment end-member is not known with accuracy, it is not likely to vary much on the small spatial scale involved in the studied crust. Instead, the detritus at this particular site is most probably characterized by a more constant composition. This suggests that the age of one piece of the crust relative to another is much better known in relative

terms that by taking the difference in the two absolute ages. Hence, we are confident that the changes in growth rate in the crust reported above and discussed below (section 5.5) are robust, at least when described in relative terms.

5.4. A record of progressive sulphate depletion

The age-depth profile is compared to profiles for carbonate $\delta^{13}\text{C}$ and carbonate mineralogy (Gontharet et al., 2007), Sr/Ca and Mg/Ca (Fig. 2). Sr/Ca and Mg/Ca ratios show opposite vertical trends, indicating a gradual downward change from aragonite to high-Mg-rich carbonate phases. A similar mineralogical trend was reported for a carbonate crust collected from the Amsterdam mud volcano in the eastern Mediterranean basin (Aloisi et al., 2002). In the absence of any microscopic evidence for re-crystallisation of aragonite into high-Mg calcite, this trend is best explained by a change in chemical conditions (Aloisi et al., 2002). Previous studies have shown that aragonite precipitation is favoured over that of high-Mg calcite at high SO_4^{2-} concentrations (e.g. Burton and Walker, 1987; Burton, 1993), whereas high-Mg carbonates generally precipitate from pore waters with low dissolved SO_4^{2-} contents, typically at the interface between methane and sulphate (Luff and Wallman, 2003; Luff et al., 2004; Gieskes et al., 2005). Our geochemical data therefore suggest that the mineralogical trend from aragonite to high-Mg carbonates in crust NL7-CC2 was induced by a progressive depletion in dissolved sulphate.

In anoxic or suboxic conditions, it is well known that U is reduced from its hexavalent to its tetravalent state and becomes insoluble. The depth profile for U concentrations across NL7-CC2 (see Table 2), indicating increasing U concentrations from top to bottom, therefore would also suggest that a gradual change in chemical conditions occurred during the formation of the crust. This is further supported by the down-crust $\delta^{13}\text{C}$ profile (Fig. 3D). Methane-rich fluids on continental margins are characterized by $\delta^{13}\text{C}$ values ($\delta^{13}\text{C}$ from ~ -110 to -30 ‰) much lower than seawater ($\delta^{13}\text{C} \sim 1$ ‰). Hence, the progressive downward depletion in carbonate ^{13}C in crust NL7-CC2 indicates an increasing contribution from AOM-derived versus seawater-derived carbon in the lower part of the crust (Gontharet et al., 2007). Overall, these data point clearly toward a progressive isolation of the growing crust from seawater

through time. This is consistent with the downward growth of the crust indicated by the U/Th chronology.

5.5. Carbonate precipitation rates

Interestingly, variations in mineralogy across crust NL7-CC2 coincide relatively well with the changes in growth rates determined from the age-depth profile (Fig. 3). In particular, the transition between aragonite and high-Mg calcite in the lower part of the crust corresponds to a shift from fast (~ 5 cm/kyr) to slow (~ 0.8 cm/kyr) period of carbonate formation (Fig. 3E). Growth rates can be converted into carbonate precipitation rates using the bulk crust density (1.6 g cm^{-3}). The carbonate precipitation rates corresponding to the three growth periods in NL7-CC2 average $\sim 6 \mu\text{mol cm}^{-2} \text{ a}^{-1}$ for the topmost part of the crust, $\sim 80 \mu\text{mol cm}^{-2} \text{ a}^{-1}$ for the middle part, and $\sim 12 \mu\text{mol cm}^{-2} \text{ a}^{-1}$ for the high-Mg carbonate part of the crust. Using dimensions commonly used in experimental studies ($\mu\text{mol m}^{-2} \text{ h}^{-1}$), those carbonate precipitation rates yield ~ 7 , 92 and $14 \mu\text{mol m}^{-2} \text{ h}^{-1}$, respectively. The average rate of precipitation estimated for the high-Mg carbonate layer ($14 \mu\text{mol m}^{-2} \text{ h}^{-1}$) is consistent with rates determined previously from laboratory experiments ($1\text{-}14 \mu\text{mol m}^{-2} \text{ h}^{-1}$; Burton and Walter, 1987; Zhong and Mucci, 1993) and numerical modeling of biogeochemical processes at cold seeps ($11 \mu\text{mol m}^{-2} \text{ h}^{-1}$; Luff and Wallmann, 2003). The average aragonite precipitation rate calculated for the middle part of the crust ($\sim 92 \mu\text{mol m}^{-2} \text{ h}^{-1}$) is in agreement with the kinetic constant derived from modeling by Luff and Wallmann ($114 \mu\text{mol m}^{-2} \text{ h}^{-1}$), but higher than experimental values ($22\text{-}41 \mu\text{mol m}^{-2} \text{ h}^{-1}$; Burton and Walter, 1987). This finding hence would confirm the existing literature indications that aragonite precipitates much faster at cold seeps than during abiotic laboratory experiments.

5.6. Controls on carbonate crust formation at cold seeps

Several parameters are known to affect carbonate formation at cold seeps, including sedimentation rates, bioturbation, bioirrigation, and upward methane fluxes (see Luff et al., 2004; Luff and Wallmann, 2004). The fact that the ~ 5000 year-old NL7-CC2 crust is still exposed on the seafloor at present suggests that particles sedimenting on the seafloor at the studied location have been eroded with time, and hence that changes in sedimentation rates have not played a significant role in controlling the formation of the crust.

At the onset of fluid seepage, an initial cm-thick layer of aragonite may precipitate relatively rapidly, in just a few hundred years (Luff et al., 2005). The same authors have suggested that subsequent development of carbonate crust is limited by high bioturbation activity. The presence of large fragments of chemosynthetic bivalves in the topmost part of NL7-CC2 crust suggests that bioturbation was active ~ 5 kyr ago, during the initial stage of carbonate precipitation (Fig. 5A). At that time, the initiation of fluid venting probably led to development of vent communities and associated bioturbation processes in the near-seafloor environment. Most likely, this initial stage of carbonate crust formation led to pore space clogging, reduced fluid venting and associated development of macro-benthos communities supported by chemosynthesis, all of which would have resulted in a significant drop of bioturbation at the studied location (Fig. 5B). It is possible that the absence of bioturbation resulted in enhanced carbonate precipitation, thereby explaining the differences in aragonite growth rates observed in the topmost layer of crust NL7-CC2, from slow (average $7 \mu\text{mol m}^2 \text{h}^{-1}$) to fast ($\sim 92 \mu\text{mol m}^2 \text{h}^{-1}$) rates.

Certainly, the development of an aragonite crust near the sediment surface would have affected the exchange of dissolved species between sediment and bottom water, leading to reduced supply of CH_4 and lower AOM rates. As a consequence, as less bicarbonate is supplied to pore water via AOM, dissolution of aragonite may start after the initial stage of carbonate crust formation. Using numerical simulations, Luff et al. (2005) suggested that aragonite dissolution may prevail over precipitation at this stage, at least temporarily. Then, after the initial aragonite layer has become thinner, higher flow velocity allows again for enhanced upward transport of methane, inducing in turn precipitation of aragonite and calcite at the base of the initial aragonite crust (Luff et al., 2005). A new maximum in AOM rates and aragonite precipitation can hence be attained, which leads to the formation of a new aragonite-rich layer, about 2000 yrs after the initial stage of carbonate precipitation (Fig. 5B). Those results from numerical modeling agree well with the mineralogical and geochemical downward changes observed in crust NL7-CC2. Therefore, the lower rates of carbonate precipitation observed for the top part of the crust could also reflect, at least to some degree, a temporary episode of aragonite dissolution that followed the initial stage of carbonate crust formation ~ 5000 years ago.

One of the most prominent results of this study is the gradual SO_4^{2-} depletion at the studied location inferred from $\delta^{13}\text{C}$, Sr/Ca and Mg/Ca data, which could result either from enhanced upward methane fluxes and/or a reduction of the dissolved sulphate transport to the base of the crust. Although a change in the upward CH_4 flux is possible, it is very likely that the downward flux of seawater sulphate has dropped with time. In carbonate-paved areas, bioirrigation is an important factor controlling the solute exchange between bottom-waters and underlying sediments, in which macrobenthic organisms actively pump water into the sediment. At the studied location, the presence of dense bushes of vestimentiferan tubeworms must have sustained an active and continuous inflow of seawater sulphate over the last thousand years, which allowed high AOM turnover and fast aragonite precipitation at the base of crust (Fig. 5B). However, with time, it is likely that the efficiency of this biological pump has decreased, most probably in response to progressive clogging due to intense carbonate formation (Fig. 5C).

6. Concluding remarks

The application of U-series to methane-derived authigenic carbonates adds unique temporal information to the study of biogeochemical processes related to anaerobic oxidation of methane (AOM) on continental margins. U-Th ages require correction for appreciable initial Th content, and we have shown that this is more appropriately performed using the U-Th composition of local sediment containing excess ^{230}Th from seawater, than with typical crustal U-Th values. Dating of a crust from the Nile deep-sea fan demonstrates clearly something previously suspected – that crusts grow downwards with time from the sediment surface – in this case over a period of ~ 5kyr. This chronology also allows carbonate precipitation rates to be estimated. Calculated rates for average aragonite formation are about six-time higher than for high-Mg calcite. In agreement with numerical studies, aragonite precipitates much faster at cold seeps than during abiotic laboratory experiments, due most probably to microbial catalysis. Our results also highlight the role played by chemosynthetic macro-benthos at cold seeps in the formation of cold seep carbonates, through transport of seawater sulphate available for AOM (i.e. bioirrigation). Comparison of $^{230}\text{Th}/\text{U}$ ages with other data (mineralogy, $\delta^{13}\text{C}$, Sr/Ca, Mg/Ca) suggests that both carbonate mineralogy

and precipitation rates are closely related to the efficiency of this biological pump through time.

Acknowledgements

The Nautinil expedition was funded by Ifremer, as part of the MEDIFLUX Project (EUROMARGINS–ESF programme). We thank the captain, the officers and crews of R/V *Atalante*, the pilots and technicians of *Nautille*, and the members of the Nautinil scientific parties for their assistance at sea. J. Etoubleau (Ifremer) is thanked for XRF data. A. Mason and N. Charnley (U. Oxford) are thanked for assistance during U/Th analyses and SEM work, respectively. Two anonymous reviewers are acknowledged for providing thoughtful and constructive reviews, which improve significantly our manuscript.

Appendix: Calculation of the proportion of the hydrogenous component in the uppermost carbonate crust sample and of its ($^{230}\text{Th}/^{232}\text{Th}$) composition

The ^{232}Th , ^{230}Th and ^{238}U budgets in the uppermost crust sample follow the mass balance equations:

$$^{232}\text{Th}_{\text{total}} = ^{232}\text{Th}_{\text{sediment}} \cdot x + ^{232}\text{Th}_{\text{hydrogenous}} \cdot y + ^{232}\text{Th}_{\text{carbonate}} \cdot z \quad (1)$$

$$^{230}\text{Th}_{\text{total}} = ^{230}\text{Th}_{\text{sediment}} \cdot x + ^{230}\text{Th}_{\text{hydrogenous}} \cdot y + ^{230}\text{Th}_{\text{carbonate}} \cdot z \quad (2)$$

$$^{238}\text{U}_{\text{total}} = ^{238}\text{U}_{\text{sediment}} \cdot x + ^{238}\text{U}_{\text{hydrogenous}} \cdot y + ^{238}\text{U}_{\text{carbonate}} \cdot z \quad (3)$$

where $^{230}\text{Th}_{\text{carbonate}}$ refers to the ^{230}Th accumulated by decay of U since the authigenic carbonate sample formed. The subscripts *sediment* and *hydrogenous* refer to the sediment and water-derived contributions, respectively, of ^{232}Th , ^{230}Th and ^{238}U . Sediment values for ^{232}Th (4.68 ppm), ^{230}Th (58 ppt) and ^{238}U (1.33 ppm) are derived from the analyses of the two studied sediments. The subscript *total* refers to the measured concentrations of ^{232}Th (0.86 ppm), ^{230}Th (17.6 ppt) and ^{238}U (4.85 ppm) in the bulk carbonate sample. x , y and z represents the proportions of sediment, hydrogenous (Fe-oxides) and authigenic carbonate fractions, respectively. Microprobe measurements of the detritus content in the uppermost carbonate sample indicate that $x \sim 0.005$ (0.5 wt%).

Assuming that $^{232}\text{Th}_{\text{hydrogenous}} = 100$ ppm (Henderson and Burton, 1999) and $^{232}\text{Th}_{\text{carbonate}} = 0$, the proportion y of the hydrogenous component incorporated in the uppermost carbonate sample can be calculated from Eqn. 1: $y \sim 0.008$ (0.8 wt%). This shows that $\sim 60\%$ of ^{232}Th in this uppermost crust sample derives from the hydrogenous component (most probably associated to the Fe-oxide coating), whereas the remaining $\sim 40\%$ of ^{232}Th derived from the sediment incorporated within the carbonate matrix.

Then, assuming that $^{238}\text{U}_{\text{hydrogenous}} = 13$ ppm (Henderson and Burton, 1999), $^{238}\text{U}_{\text{carbonate}}$ can be inferred using Eqn. 3: $^{238}\text{U}_{\text{carbonate}} \sim 4.80$ ppm.

Based on the $^{230}\text{Th}/\text{U}$ age profile for crust NL7-CC2, it can be reasonably argued that the uppermost part of the crust formed about 5000 years ago. Using this age, one can use the ^{230}Th age equation (Eqn. 4) to deduce $^{230}\text{Th}_{\text{carbonate}} \sim 4.2$ ppt.

$$(^{230}\text{Th}_{\text{carbonate}} / ^{238}\text{U}_{\text{carbonate}}) = 1 - e^{-\lambda_{230}t} + (\delta^{234}\text{U}_m / 1000) \cdot (\lambda_{230} / (\lambda_{230} - \lambda_{234})) \cdot (1 - e^{-(\lambda_{230} - \lambda_{234})t}) \quad (4)$$

The value obtained for $^{230}\text{Th}_{\text{carbonate}}$ can be inserted in Eqn. 2 to infer $^{230}\text{Th}_{\text{hydrogenous}} \sim 1650$ ppt, and finally, $(^{230}\text{Th}/^{232}\text{Th})_{\text{hydrogenous}} = 3.1$.

References

- Aloisi, G., Pierre, C., Rouchy, J.-M., Foucher, J.-P., Woodside, J., the MEDINAUT Scientific Party, 2000. Methane-related authigenic carbonates of eastern Mediterranean Sea mud volcanoes and their possible relation to gas hydrate destabilisation. *Earth Planet. Sci. Lett.* 184, 321-338.
- Aloisi, G., Bouloubassi, I., Heijs, S.K., Pancost, R.D., Pierre, C., Sinninghe Damsté, J.S., Gottschal, J.C., Forney, L.J., Rouchy, J.-M., 2002. CH₄-consuming microorganisms and the formation of carbonate crusts at cold seeps. *Earth Planet. Sci. Lett.* 203, 195-203.
- Bayon, G., Pierre, C., Etoubleau, J., Voisset, M., Cauquil, E., Marsset, T., Sultan, N., Le Drezen, E., Fouquet, Y., 2007. Sr/Ca and Mg/Ca ratios in Niger Delta sediments: Implications for authigenic carbonate genesis in cold seep environments. *Mar. Geol.* 241, 93-109.
- Bayon, G., Loncke, L., Dupré, S., Caprais, J.-C., Ducassou, E., Duperron, S., Etoubleau, J., Foucher, J.-P., Fouquet, Y., Gontharet, S., Henderson, G.M., Huguen, C., Klaucke, I., Mascle, J., Migeon, S., Olu-Le Roy, K., Ondréas, H., Pierre, C., Sibuet, M., Stadnitskaia, A., Woodside J., Fluid seepage on an unstable margin: The case of the Centre Nile fan. *Mar. Geol.* In press.
- Bischoff, J.L., Fitzpatrick, J.A., 1991. U-series of impure carbonates: An isochron technique using total-sample dissolution. *Geochim. Cosmochim. Acta* 55, 543–554.
- Bohrmann, G., Meinert, J., Suess, E., Torres, M., 1998. Authigenic carbonates from the Cascadia subduction zone and their relation to gas hydrate stability. *Geology* 26, 647-650.
- Burton, E.A., Walker, L.M., 1987. Relative precipitation rates of aragonite and Mg calcite from seawater: Temperature or carbonate ion control? *Geology* 15, 111-114.
- Burton, E.A., 1993. Controls on marine carbonate cement mineralogy: review and reassessment. *Chem. Geol.* 105, 163-179.
- Cheng, H., Edwards, R.L., Hoff, J., Gallup, C.D., Richards, D.A., Asmeron, Y., 2000. The half-lives of ²³⁴U and ²³⁰Th. *Chem. Geol.* 169, 17-33.

597 Cochran, J.K., Carey, A.E., Sholkovitz, E.R., Surprenant, L.D., 1986. The
 598 geochemistry of uranium and thorium in coastal marine sediments and sediment
 599 pore waters. *Geochim. Cosmochim. Acta* 50, 663–680.

600 Condie, K.C., 1993. Chemical composition and evolution of the upper continental
 601 crust: contrasting results from surface samples and shales. *Chem. Geol.* 104, 1-37.

602 Dosseto, A., Turner, S.P., Douglas, G.B., 2006. Uranium-series isotopes in colloids
 603 and suspended sediments: Timescale for sediment production and transport in the
 604 Murray–Darling River system. *Earth Planet. Sci. Lett.* 246, 418-431.

605 Dosseto, A., Bourdon, B., Gaillardet, J., Maurice-Bourgoin, L., Allègre, C.J., 2006.
 606 Weathering and transport of sediments in the Bolivian Andes: Time constraints
 607 from uranium-series isotopes. *Earth Planet. Sci. Lett.* 248, 759-771.

608 Edwards, R.L., Chen, J.H., Wasserburg, G.R., 1986. ^{238}U - ^{234}U - ^{230}Th - ^{232}Th systematics
 609 and the precise measurement of time over the past 500,000 years. *Earth Planet. Sci.*
 610 *Lett.* 81, 175-192.

611 Edwards, R.L., Gallup, C.D., Cheng, H., 2003. Uranium-series dating of marine and
 612 lacustrine carbonates. *Rev. Min. Geochem.* 52, 363-405.

613 Gariépy, C., Ghaleb, B., Hillaire-Marcel, C., Mucci, A., Vallières, S., 1993. Early
 614 diagenetic processes in Labrador Sea sediments: Uranium-isotope geochemistry.
 615 *Can. J. Earth Sci.* 31, 29–37.

616 Gieskes, J., Mahn, C., Day, S., Martin, J.B., Greinert, J., Rathburn, T., MacAdoo, B.,
 617 2005. A study of the chemistry of pore fluids and authigenic carbonates in methane
 618 seep environments: Kodiak Trench, Hydrate Ridge, Monterey Bay, and Eel River
 619 Basin. *Chem. Geol.* 220, 329-345.

620 Gontharet, S., Pierre, C., Blanc-Valleron, M.M., Rouchy, J.M., Fouquet, Y., Bayon, G.,
 621 Foucher, J.P., Woodside, J., Mascle, J., the Nautinil scientific party, 2007. Nature
 622 and origin of the diagenetic carbonate crusts and concretions from mud volcanoes
 623 and pockmarks of the Nile deep-sea fan (eastern Mediterranean sea). *Deep-Sea*
 624 *Research part II*, in press.

625 Greinert, J., Bohrmann, G., Suess, E., 2001. Gas hydrate-associated carbonates and
 626 methane venting at Hydrate Ridge: Classification, distribution and origin of
 627 carbonate lithologies. In: Paull, C.K., Dillon, W.P. (Ed.), *Natural Gas Hydrates:*

628 Occurrence, Distribution and Detection, American Geophysical Union, Vol. 124,
629 pp. 99-113.

630 Greinert, J., Bohrmann, G., Elvert, M., 2002. Stromatolitic fabric of authigenic
631 carbonate crusts: result of anaerobic methane oxidation at cold seeps in 4,850 water
632 depth. *Int. J. Earth. Sci.* 91, 698-711.

633 Henderson, G.M. and Burton, K.W., 1999. Using ($^{234}\text{U}/^{238}\text{U}$) to assess diffusion rates of
634 isotopic tracers in Mn crusts. *Earth Planet. Sci. Lett.*, 170, 169-179.

635 Henderson, G.M., Slowey, N.C., Haddadluid, G.A., 1999. Fluid flow through
636 carbonate platforms: constraints from $^{234}\text{U}/^{238}\text{U}$ and Cl^- in Bahamas pore. *Earth*
637 *Planet. Sci. Lett.* 169, 99-111.

638 Henderson, G.M., Heinze, C., Anderson, R.F. and Winguth, A.M.E., 1999. Global
639 distribution of the ^{230}Th flux to ocean sediments constrained by GCM modelling.
640 *Deep Sea Research*, 46, 1861-1893.

641 Henderson, G.M., Slowey, N.C., Fleisher, M.Q., 2001. U-Th dating of carbonate
642 platform and slope sediments. *Geochim. Cosmochim. Acta* 65, 2757-2770.

643 Hovland, M., Talbot, M.R., Qvale, H., Olaussen, S., Aasberg, L. 1987. Methane-
644 related carbonate cements in pockmarks of the North Sea. *J. Sedim. Petrol.* 57,
645 881-892.

646 Lalou, C., Fontugne, M., Lallemand, S.E., Lauriat-Rage, A., 1992. Calyptogena-
647 cemented rocks and concretions from the eastern part of Nankai accretionary prism:
648 Age and geochemistry of uranium. *Earth Planet. Sci. Lett.* 109, 419-429.

649 Lin, J.C., Broecker, W.S., Anderson, R.F., Hemming, S., Rubenstone, J.L., Bonani, G.,
650 1996. New $^{230}\text{Th}/\text{U}$ and ^{14}C ages from Lake Lahontan carbonates, Nevada, USA,
651 and a discussion of the origin of initial thorium. *Geochim. Cosmochim. Acta* 60,
652 2817-2832.

653 Loncke, L., Gaullier, V., Mascle, J., Vendeville, B., Camera, L., 2006. The Nile deep-
654 sea fan : An example of interacting sedimentation, salt tectonics, and inherited
655 subsalt paleotopographic features. *Marine Petroleum Geology* 23, 297-315.

656 Ludwig, K.R., 2003. Using Isoplot/Ex, Version 3, A geochronological toolkit for
657 Microsoft Excel: Berkeley Geochronology Ctr. Spec. Pub. 4.

658 Ludwig, K.R., Paces, J. B., 2002. Uranium-series dating of pedogenic silica and
659 carbonate, Crater Flat, Nevada. *Geochim. Cosmochim. Acta* 66, 487-506.

660 Luff, R., Wallmann, K., 2003. Fluid flow, methane fluxes, carbonate precipitation and
 661 biogeochemical turnover in gas hydrate-bearing sediments at Hydrate Ridge,
 662 Cascadia Margin: numerical modelling and mass balances, *Geochim. Cosmochim.*
 663 *Acta* 67, 3403–3421.

664 Luff, R., Wallmann, K., Aloisi, G., 2004. Numerical modeling of carbonate crust
 665 formation at cold vent sites: significance for fluid and methane budgets and
 666 chemosynthetic biological communities. *Earth Planet. Sci. Lett.* 221, 337–353.

667 Luff, R., Greinert, J., Wallmann, K., Klauke, I., Suess, E., 2005. Simulation of long-
 668 term feedbacks from authigenic carbonate crust formation at cold vent sites. *Chem.*
 669 *Geol.* 216, 157-174.

670 Luo, S.D., Ku, T.-L., 1991. U-series isochron dating: A generalized method employing
 671 total-sample dissolution. *Geochim. Cosmochim. Acta* 55, 555–564.

672 Mazzini, A., Ivanov, M. K., Parnell, J., Stadnitskaia, A., Cronin, B.T., Poludetkina, E.,
 673 Mazurenko, L., van Weering, T.C.E., 2004. Methane-related authigenic carbonates
 674 from the Black Sea: geochemical characterisation and relation to seeping fluids.
 675 *Mar. Geol.* 212, 153-181.

676 Michaelis, W., Seifert, R., Nauhaus, K., Treude, T., Thiel, V., Blumenberg, M., Knittel,
 677 K., Geiseke, A., Peterknecht, K., Pape, T., Boetius, A., Amann, R., Jorgensen, B.B.,
 678 Widdel, F., Peckmann, J., Pimenov, N.V., Gulin, M.B., 2002. Microbial reefs in
 679 the Black Sea fueled by anaerobic oxidation of methane. *Science* 297, 1013-1015.

680 Paull, C.K., Chanton, J.P., Neumann, A.C., Coston, J.A., Martens, C.S., 1992.
 681 Indicators of methane-derived carbonates and chemosynthetic organic carbon
 682 deposits: examples from the Florida escarpment. *J. Soc. Sediment. Geol. Palaios* 7,
 683 361-375.

684 Reitner, J., Peckmann, J., Blumenberg, M., Michaelis, W., Reimer, A., Thiel, V., 2005.
 685 Concretionary methane-seep carbonates and associated microbial communities in
 686 Black Sea sediments. *Palaeog., Palaeoclim. Palaeoecol.* 227, 18-30.

687 Ritger, S., Carson, B., Suess, E., 1987. Methane-derived authigenic carbonates formed
 688 by subduction-induced pore-water expulsion along the Oregon/Washington margin.
 689 *Geol. Soc. Am. Bull.* 98, 147-156.

690 Robinson, L.F., Henderson, G.M., Slowey, N.C., 2002. U–Th dating of marine isotope
 691 stage 7 in Bahamas slope sediments. *Earth Planet. Sci. Lett.* 196, 175-187.

692 Robinson, L.F., Belshaw, N.S., Henderson, G.M., 2004. U and Th concentrations and
 693 isotope ratios in modern carbonates and waters from the Bahamas. *Geochim.*
 694 *Cosmochim. Acta* 68, 1777-1789.

695 Roy-Barman, M., Coppola, L., Souhaut, M., 2002. Thorium isotopes in the western
 696 Mediterranean Sea: an insight into the marine particle dynamics. *Earth Planet. Sci.*
 697 *Lett.* 196, 161-174.

698 Stadnitskaia, A., Muyzer, G., Abbas, B., Coolen, M.J.L., Hopmans, E.C., Bass, M., van
 699 Weering, T.C.E., Ivanov, M.K., Poludetkina, E., Sinninghe Damsté, J.S., 2005.
 700 Biomarker and 16S rDNA evidence for anaerobic oxidation of methane and related
 701 carbonate precipitation in deep-sea mud volcanoes of the Sorokin Trough. *Mar.*
 702 *Geol.* 217, 67-96.

703 Taylor, S.R., McLennan, S.M., 1985. The continental crust: Its composition and
 704 evolution. Blackwell, Oxford, 312 pp.

705 Teichert, B.M.A., Eisenhauer, A., Bohrmann, G., Haase-Schramm, A., Bock, B., Linke,
 706 P., 2003. U/Th systematics and ages of authigenic carbonates from Hydrate Ridge,
 707 Cascadia Margin: recorders of fluid flow variations. *Geochim. Cosmochim. Acta* 67,
 708 3845-3857.

709 Vigier, N., Bourdon, B., Turner, S., Allègre, C.J., 2001. Erosion timescales derived
 710 from U-decay series measurements in rivers. *Earth Planet. Sci. Lett.* 193, 549-563.

711 Zhong, S., Mucci, A., 1993. Calcite precipitation in seawater using a constant addition
 712 technique: A new overall reaction kinetic expression. *Geochim. Cosmochim. Acta*
 713 57, 1409-1417.

Table captions

Table 1

<DL means concentration lower than the instrumental detection limit.

Table 2

Depths indicated for samples correspond to centimetres below the surface of the crust. Round brackets denote activity ratio. All calculations have used the half-lives measured by Cheng et al. (2000).

Table 3

Depths indicated for samples correspond to centimetres below the top of the crust. Initial $\delta^{234}\text{U}$ represents the deviation in permil of ($^{234}\text{U}/^{238}\text{U}$) from its secular equilibrium value of 1.000, at the time T of carbonate precipitation, with initial $\delta^{234}\text{U} = [\{ (^{234}\text{U}/^{238}\text{U})_{\text{T}} / (^{234}\text{U}/^{238}\text{U})_{\text{equ}} \} - 1] \times 10^3$. Measured values (see Table 2) are corrected for detrital contamination and decay of excess ^{234}U since sample formation. One sample (0.0cm) is rejected as meaningful age based on the presence of significant seawater ^{230}Th (see text for details), and is shown in italics. Other calculated ages are considered reliable. All calculations have used the half-lives measured by Cheng et al. (2000).

Figure captions

Figure 1

Shaded bathymetric map of the Central Nile deep-sea fan (Loncke et al., 2006), and location of the studied carbonate crust. Crust NL7-CC2 was collected from a carbonate-paved area, at an active zone of fluid venting located at ~ 1650 m water depth.

Figure 2

Description of carbonate crust NL7-CC2. (A) Seafloor bottom photograph showing sampling with the *Nautilie* submersible. Upon recovery, numerous living vestimentiferan tubeworms were observed anchored at the base of the crust. (B) Cross-section. Crust NL7-CC2 is a highly porous carbonate-cemented mudstone covered by a fine layer of Fe-oxyhydroxides. Numerous fragments of bivalve shells are observed in the upper ~1-cm of the crust. Fibrous aragonite is present in open pore spaces, either in cracks or inside the cavities of biogenic components. Crust NL7-CC2 is dominated by aragonite, but exhibits mineralogical variability, characterized by a gradual enrichment in high-Mg carbonate phases from top to bottom (Gontharet et al., 2007). The areas of the crust sampled for U-Th analysis are shown as white-filled squares (hand-drilled samples), green-filled rectangles (micromilled samples). The micromilled sample at 0.0 cm (crossed red-filled rectangle) was rejected as meaningful age based on the presence of significant seawater ^{230}Th (see text for details).

Figure 3

High-resolution profiles for A) Sr/Ca ratios; B) Mg/Ca ratios; C) detritus contents (wt%); D) $\delta^{13}\text{C}$ (‰ PDB), Gontharet et al. (2007); and E) $^{230}\text{Th}/\text{U}$ ages (kyr BP) across NL7-CC2 crust. A), B), C) The small empty squares correspond to electron microprobe data, and the larger infilled squares to XRF analyses of bulk carbonate crust samples. Detrital contents were calculated by summing contents (wt %) of XRF data for K_2O , Fe_2O_3 , SiO_2 , TiO_2 and Al_2O_3 (see Table 1). Below the aragonite-rich upper crust layer, the frequency of high Mg/Ca values increases progressively with depth, indicating enhanced contribution from high-Mg carbonate phases. Detrital contents in crust NL7-CC2 can be as high as ~ 12 wt%, increasing progressively with depth. D) The progressive downward depletion in carbonate ^{13}C in crust NL7-CC2 indicates an increasing contribution from AOM-derived versus seawater-derived carbon in the lower part of the crust (Gontharet et al., 2007). E) The $^{230}\text{Th}/\text{U}$ ages vary from $\sim 4.9 \pm 1.2$ ka in the topmost part of the crust to $\sim 0.8 \pm 1.3$ ka at its base, indicating that the crust has grown downward. Three growth periods can be distinguished from top to bottom (dashed lines), with average growth rates of ~ 0.4, 5 and 0.8 cm/kyr, respectively (thick lines). Those growth variations are accompanied by changes in carbonate mineralogy (see Sr/Ca and Mg/Ca profiles) and fluid composition (see $\delta^{13}\text{C}$ values). The vertical error bars shown in panels D) and E)

correspond to sample thickness. The horizontal error bars are 2sd uncertainties on isochron ages.

Figure 4

A) Rosholt isochron diagram for bulk and micromilled carbonate samples (crust NL7-CC2). Isochron ages are calculated from the slope of the isochrons, using a sediment end-member defined as the average of the two studied sediments. The values for the sediment end-member are $(^{230}\text{Th}/^{232}\text{Th}) = 2.30 \pm 0.47$ (2SD) and $(^{238}\text{U}/^{232}\text{Th}) = 0.87 \pm 0.02$ (2SD). The dashed line represents the equiline. Note the large error bars on $(^{238}\text{U}/^{232}\text{Th})$ ratios for samples drilled at 0.4 cm, 0.9 cm and 2.8 cm depth below the crust surface, which prevent calculation of reliable ages. B) Comparison of $(^{230}\text{Th}/^{232}\text{Th})$ vs. $(^{238}\text{U}/^{232}\text{Th})$ ratios of cold seep carbonates from different settings, including our carbonate crust samples from the Nile deep-sea fan, carbonate nodules collected in hydrate-bearing sediments from methane seeps off Joetsu (Eastern Margin of Japan Sea; Watanabe et al., 2008), and aragonite chemohermes recovered on the seafloor at the Hydrate Ridge (Cascadia Margin; Teichert et al., 2003). Note that the $(^{238}\text{U}/^{232}\text{Th})$ ratios decrease from the Hydrate Ridge chemoherm carbonates (from ~ 100 to 10000), the crust samples from the Nile margin (from ~ 15 to 175; this study), and the carbonate nodules from the Japan Sea (from ~ 4 to 16), which may reflect, at least partly, an increasing contamination by detrital material during carbonate precipitation.

Figure 5

Schematic diagram for the mode of formation of the studied carbonate crust, integrating mineralogical and geochemical data, and calculated $^{230}\text{Th}/\text{U}$ ages. A) Stage 1 (from $\sim 5 \pm 1$ to 3 ± 1 kyr BP) - onset of fluid venting at the studied location leading to development of chemosynthetic communities on the seafloor and aragonite precipitation. Aragonite precipitates near the seafloor, cementing shell fragments of chemosynthetic bivalves. At this stage, the formation of a cm-thick aragonite crust can reduce the exchange of dissolved species between sediment and bottom water, leading to reduced AOM rates and, possibly, to partial aragonite dissolution. B) Stage 2 (from $\sim 3 \pm 1$ to 2 ± 1 kyr BP) – rapid growth of the carbonate crust. The absence of significant bioturbation and an efficient supply of seawater sulphate at the base of the

810 crust via vestimentiferan tubeworms (bioirrigation), lead to high rates of AOM
811 (anaerobic oxidation of methane) turnover promoting fast carbonate precipitation
812 (mainly aragonite). C) Stage 3 (from $\sim 2 \pm 1$ kyr BP to present) – reduced rates of
813 carbonate formation. The bottom part of the crust becomes isolated from seawater,
814 leading to reduced supply of sulphate by bioirrigation. The sulphate depletion at the
815 base of the crust induces lower AOM rates and preferential precipitation of high-Mg
816 calcite over aragonite.

Table 1. XRF major element composition of bulk carbonate and sediment samples

Sample	SiO ₂ %	Al ₂ O ₃ %	Fe ₂ O ₃ %	MnO %	MgO %	CaO %	Na ₂ O %	K ₂ O %	TiO ₂ %	P ₂ O ₅ %	SO ₄ %	LOI %	Sr ppm	Total
NL7-CC2 crust (N32°31.61', E30°21.16', 1686 m water depth)														
0-1cm	1.73	0.74	0.31	0.004	0.49	50.73	0.33	0.03	0.05	0.01	0.17	43.69	5708	98.84
1-2 cm	3.13	1.21	0.44	<DL	0.53	49.22	0.44	0.06	0.08	0.04	0.24	42.80	6382	98.82
2-3 cm	3.84	1.55	0.65	<DL	1.07	48.20	0.44	0.08	0.09	0.03	0.61	41.89	6584	99.12
3-4 cm	4.27	1.73	0.73	<DL	1.39	47.26	0.40	0.09	0.10	0.03	0.65	41.57	6343	98.86
4-5.5 cm	7.55	3.14	1.54	<DL	3.06	41.94	0.46	0.17	0.19	0.01	1.36	38.96	5497	98.92
NL7-BC1 sediment (N32°30.50', E30°23.09', 1623 m water depth)														
	20.56	7.00	3.11	0.10	3.43	31.95	0.71	0.26	0.41	0.10	0.90	30.97	1248	99.51
NL14-PC1 sediment (N32°38.33', E29°55.80', 2116 m water depth)														
	24.21	8.21	4.28	0.07	2.96	27.69	1.19	0.32	0.54	0.13	0.54	29.67	1132	99.81

Table 2. Measured U-Th data for sediment and carbonate samples

Sample	Description	Weight (mg)	²³⁸ U (ppm) ± 2σ	²³² Th (ppb) ± 2σ	(²³⁴ U/ ²³⁸ U) ± 2σ	(²³⁰ Th/ ²³² Th) ± 2σ	(²³⁸ U/ ²³² Th) ± 2σ
<u>Sediments</u>							
NL14-PC1		51.43	1.420 ± 0.002	4939.5 ± 18.5	1.025 ± 0.002	2.48 ± 0.01	0.878 ± 0.003
NL7-BC1		50.82	1.261 ± 0.002	4214.1 ± 13.1	1.041 ± 0.002	2.17 ± 0.01	0.914 ± 0.003
	replicate	327.7	1.239 ± 0.002	4634.0 ± 17.2	1.053 ± 0.002	2.12 ± 0.02	0.817 ± 0.003
<u>NL7-CC2 carbonate crust</u>							
0.0 cm	bulk	166.6	4.85 ± 0.01	861.3 ± 2.2	1.143 ± 0.002	3.83 ± 0.01	17.20 ± 0.05
0.1 cm	micromilled	1.14	4.05 ± 0.07	228.5 ± 29.4	1.138 ± 0.003	5.47 ± 0.17	54.2 ± 7.0
0.4 cm	micromilled	1.06	3.29 ± 0.06	115.8 ± 44.9	1.128 ± 0.009	6.49 ± 0.55	86.9 ± 33.7
0.9 cm	micromilled	1.06	1.67 ± 0.03	29.1 ± 4.1	1.132 ± 0.009	11.54 ± 0.41	174.9 ± 24.7
1.0 cm	bulk	43.48	8.40 ± 0.01	885.7 ± 3.7	1.141 ± 0.002	3.10 ± 0.01	28.96 ± 0.13
2.2 cm	micromilled	0.95	10.44 ± 0.22	697.0 ± 4.0	1.142 ± 0.003	3.88 ± 0.05	45.73 ± 1.00
2.5 cm	micromilled	0.56	8.79 ± 0.31	689.1 ± 8.1	1.137 ± 0.005	3.53 ± 0.05	38.95 ± 1.47
2.5 cm	bulk	111.0	12.85 ± 0.02	1323.6 ± 4.6	1.144 ± 0.002	2.91 ± 0.01	29.65 ± 0.11
	replicate	466.1	12.29 ± 0.02	1383.7 ± 4.3	1.144 ± 0.002	2.81 ± 0.04	27.12 ± 0.09
2.8 cm	micromilled	0.82	5.37 ± 0.13	202.0 ± 69.6	1.129 ± 0.009	5.25 ± 0.25	81.2 ± 28.0
3.6 cm	micromilled	1.50	8.31 ± 0.11	583.9 ± 8.4	1.140 ± 0.003	3.37 ± 0.12	43.46 ± 0.85
4.3 cm	micromilled	1.37	10.62 ± 0.16	956.8 ± 40.0	1.142 ± 0.003	3.14 ± 0.08	33.89 ± 1.50
5.0 cm	bulk	502.8	20.85 ± 0.03	2141.9 ± 4.8	1.147 ± 0.002	2.58 ± 0.04	31.14 ± 0.10
5.5 cm	bulk	103.0	20.82 ± 0.03	2044.6 ± 5.8	1.144 ± 0.002	2.57 ± 0.01	29.69 ± 0.08

Table 3. Activity ratios used for age calculation and U-Th ages for carbonate samples

Sample	$(^{232}\text{Th}/^{238}\text{U})$ $\pm 2\sigma$	$(^{230}\text{Th}/^{238}\text{U})$ $\pm 2\sigma$	$(^{234}\text{U}/^{238}\text{U})$ $\pm 2\sigma$	Corrected U-Th age (ka) $\pm 2\sigma$	Initial $\delta^{234}\text{U}$ (‰) $\pm 2\sigma$
<u>Sediment end-member</u>					
	1.149 \pm 0.029	2.65 \pm 0.47	1.036 \pm 0.030		
<u>NL7-CC2 carbonate crust</u>					
0.0 cm	0.0581 \pm 0.0002	0.2224 \pm 0.0010	1.143 \pm 0.002	9.1 \pm 2.5	153 \pm 2
0.1 cm	0.0185 \pm 0.0024	0.0917 \pm 0.0083	1.138 \pm 0.003	4.9 \pm 1.2	142 \pm 2
0.4 cm	0.0115 \pm 0.0045	0.0624 \pm 0.0181	1.128 \pm 0.005	3.5 \pm 2.1	130 \pm 9
0.9 cm	0.0057 \pm 0.0017	0.0423 \pm 0.0124	1.132 \pm 0.005	2.8 \pm 1.3	134 \pm 9
1.0 cm	0.0345 \pm 0.0001	0.1053 \pm 0.0005	1.141 \pm 0.002	2.5 \pm 1.4	145 \pm 2
2.2 cm	0.0219 \pm 0.0001	0.0805 \pm 0.0009	1.142 \pm 0.003	2.95 \pm 0.88	145 \pm 3
2.5 cm	0.0257 \pm 0.0003	0.0817 \pm 0.0013	1.137 \pm 0.005	2.2 \pm 1.0	140 \pm 5
2.5 cm	0.0337 \pm 0.0001	0.0976 \pm 0.0003	1.144 \pm 0.002	2.0 \pm 1.4	148 \pm 2
replicate	0.0369 \pm 0.0001	0.1034 \pm 0.0004	1.144 \pm 0.002	1.8 \pm 1.5	148 \pm 2
2.8 cm	0.0123 \pm 0.0042	0.0548 \pm 0.0085	1.129 \pm 0.005	2.6 \pm 1.4	131 \pm 9
3.6 cm	0.0230 \pm 0.0004	0.0741 \pm 0.0012	1.140 \pm 0.003	2.06 \pm 0.93	142 \pm 3
4.3 cm	0.0295 \pm 0.0013	0.0896 \pm 0.0054	1.142 \pm 0.003	2.1 \pm 1.3	144 \pm 3
5.0 cm	0.0337 \pm 0.0001	0.0862 \pm 0.0004	1.144 \pm 0.002	0.8 \pm 1.3	150 \pm 2
5.5 cm	0.0321 \pm 0.0001	0.0827 \pm 0.0003	1.147 \pm 0.002	0.8 \pm 1.3	148 \pm 2

Figure1

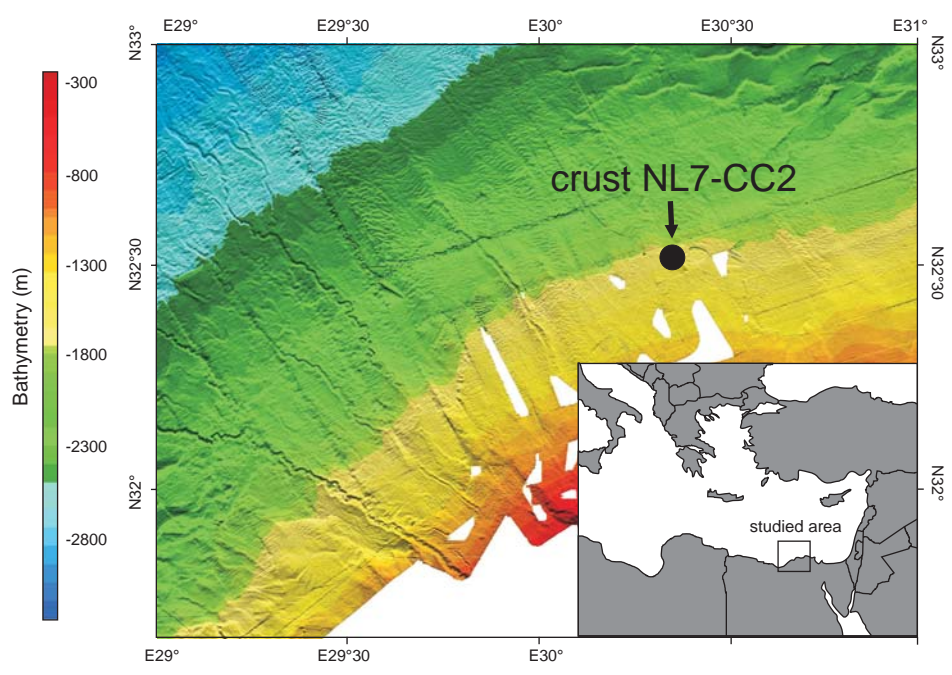


Fig1 (in colour)

Figure2

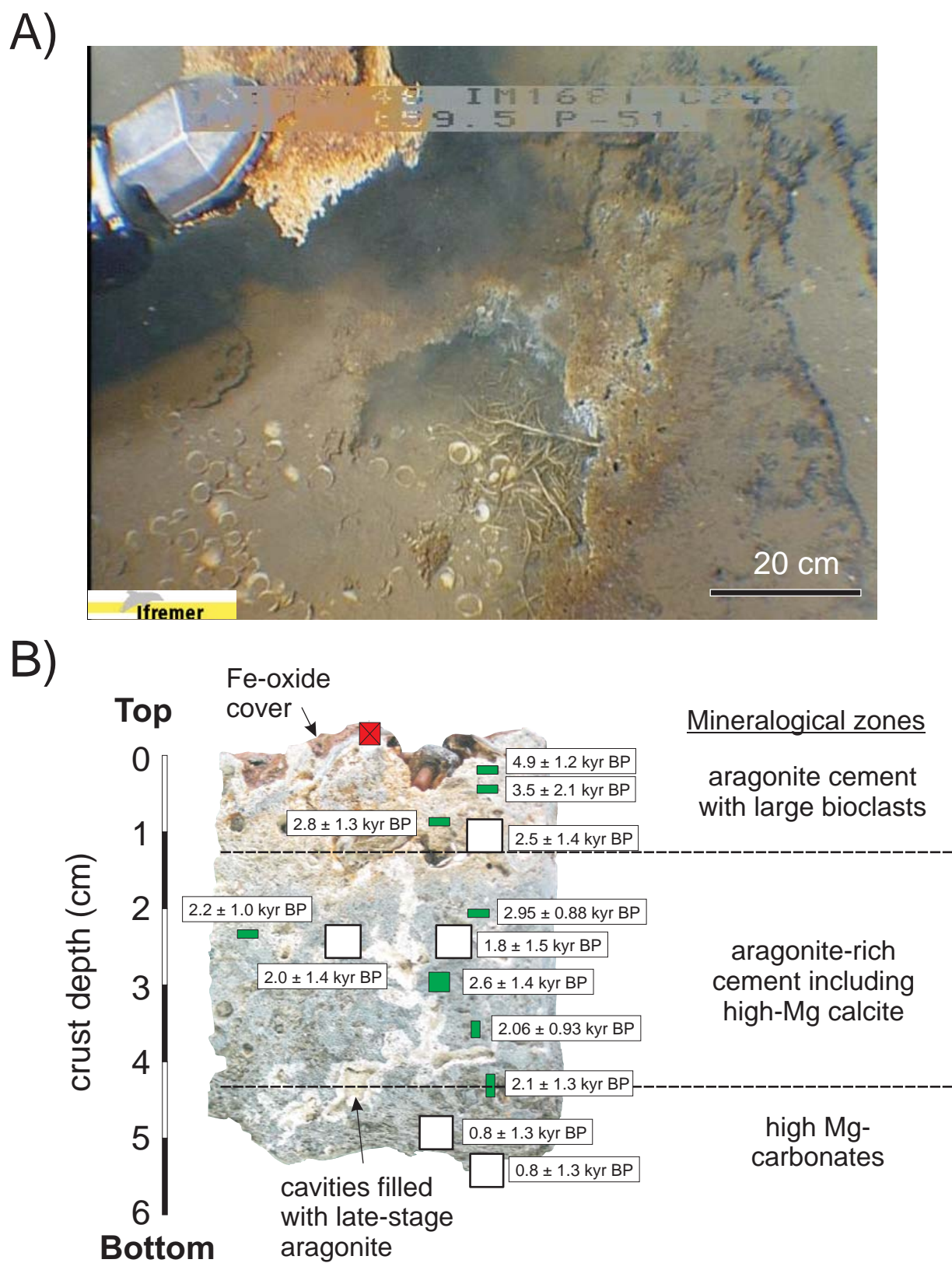


Fig. 2 (in colour in print)

Figure3

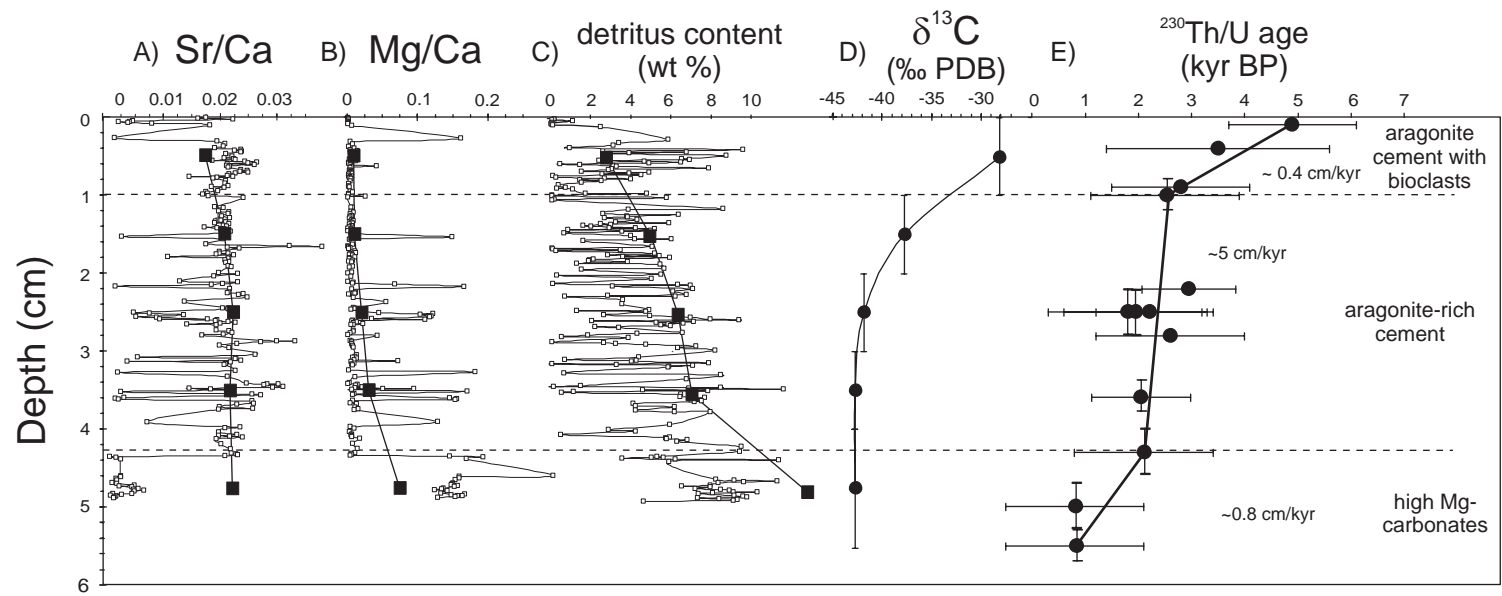


Fig. 3

Figure4

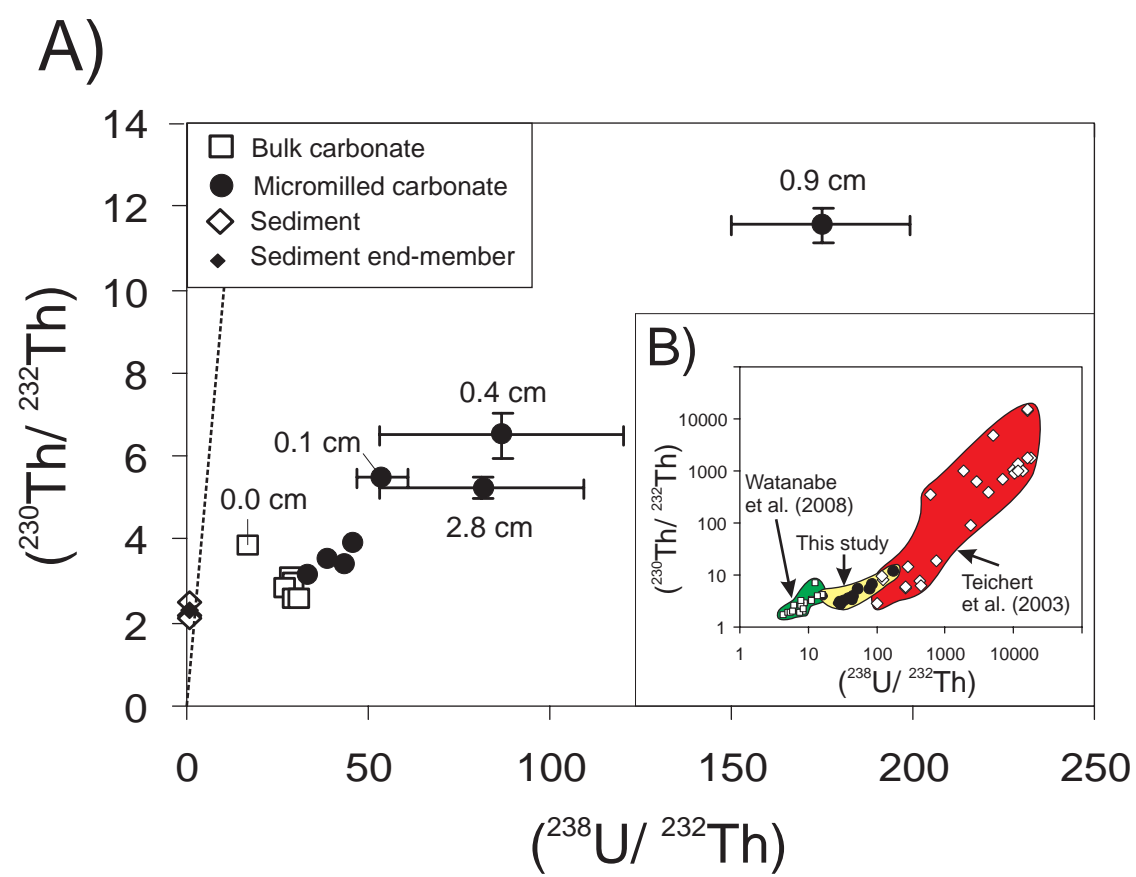


Fig. 4

Figure5

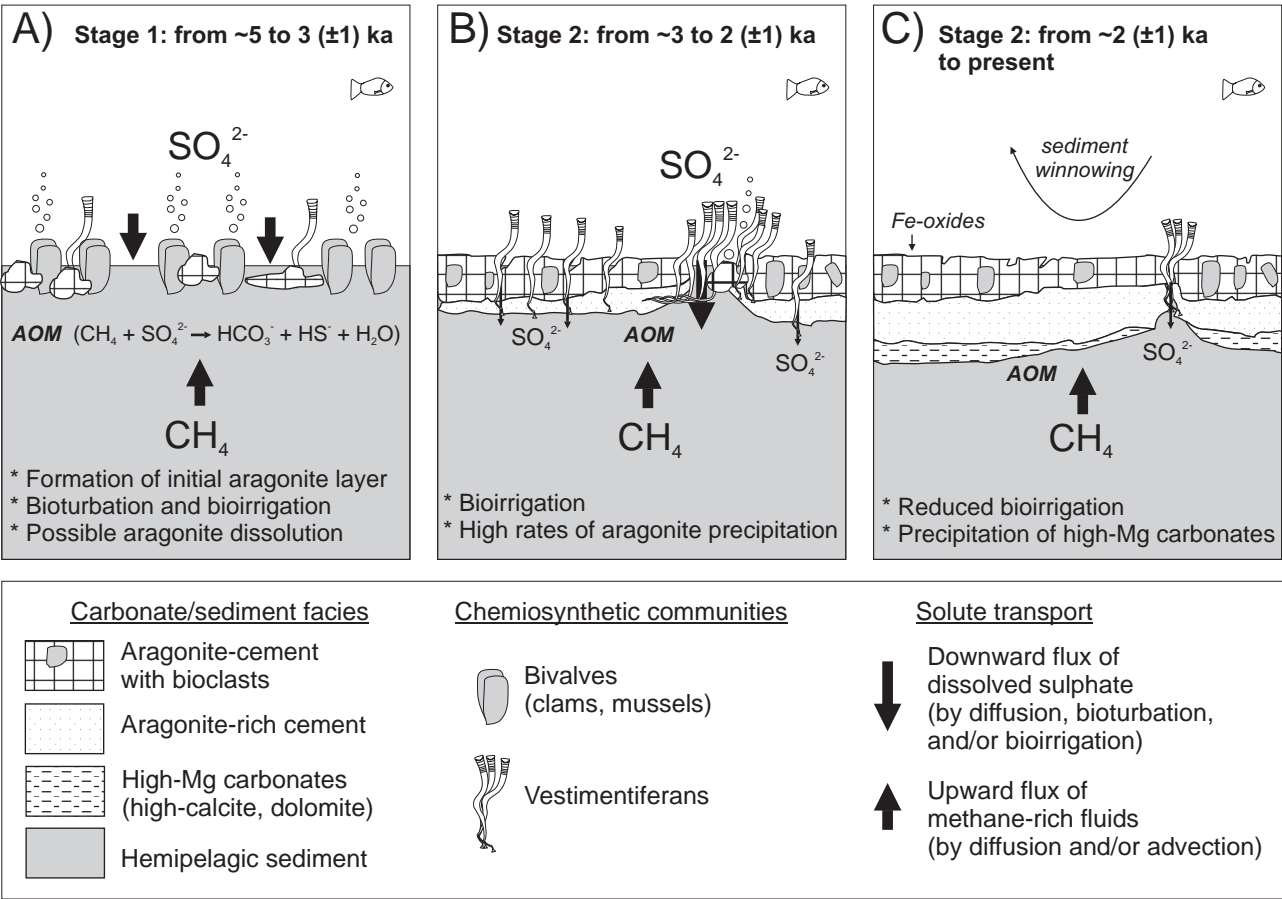


Fig. 5